2003

An Operational Remote Sensing Algorithm of Land Surface Evaporation

Kenlo Nishida

Ramakrishna R. Nemani

Steven W. Running
University of Montana - Missoula, steven.running@umontana.edu

Joseph M. Glassy

JOURNAL OF GEOPHYSICAL RESEARCH, VOL. 108, NO. D9, 4270, doi:10.1029/2002JD002062, 2003

An operational remote sensing algorithm of land surface evaporation

Kenlo Nishida
Institute of Agricultural and Forest Engineering, University of Tsukuba, Tsukuba, Japan

Ramakrishna R. Nemani and Steven W. Running
Numerical Terradynamic Simulation Group (NTSG), School of Forestry, University of Montana, Missoula, Montana, USA

Joseph M. Glassy
Lupine Logic, Inc., Missoula, Montana, USA

Received 5 January 2002; revised 17 October 2002; accepted 27 January 2003; published 7 May 2003.

[1] Partitioning of solar energy at the Earth surface has significant implications in climate dynamics, hydrology, and ecology. Consequently, spatial mapping of energy partitioning from satellite remote sensing data has been an active research area for over two decades. We developed an algorithm for estimating evaporation fraction (EF), expressed as a ratio of actual evapotranspiration (ET) to the available energy (sum of ET and sensible heat flux), from satellite data. The algorithm is a simple two-source model of ET. We characterize a landscape as a mixture of bare soil and vegetation and thus we estimate EF as a mixture of EF of bare soil and EF of vegetation. In the estimation of EF of vegetation, we use the complementary relationship of the actual and the potential ET for the formulation of EF. In that, we use the canopy conductance model for describing vegetation physiology. On the other hand, we use "VI-T_s" (vegetation index-surface temperature) diagram for estimation of EF of bare soil. As operational production of EF globally is our goal, the algorithm is primarily driven by remote sensing data but flexible enough to ingest ancillary data when available. We validated EF from this prototype algorithm using NOAA/AVHRR data with actual observations of EF at AmeriFlux stations (standard error $\cong$ 0.17 and $R^2 \cong 0.71$). Global distribution of EF every 8 days will be operationally produced by this algorithm using the data of MODIS on EOS-PM (Aqua) satellite. *INDEX TERMS:* 1818 Hydrology: Evapotranspiration; 3322 Meteorology and Atmospheric Dynamics: Land/atmosphere interactions; 3360 Meteorology and Atmospheric Dynamics: Remote sensing; *KEYWORDS:* MODIS, Aqua, evapotranspiration

Citation: Nishida, K., R. R. Nemani, S. W. Running, and J. M. Glassy, An operational remote sensing algorithm of land surface evaporation, *J. Geophys. Res.*, *108*(D9), 4270, doi:10.1029/2002JD002062, 2003.

1. Introduction

[2] Accurate characterization of evapotranspiration (ET, or latent heat flux; in this paper, in W m^{-2}) is essential for understanding climate dynamics and the terrestrial ecosystem productivity [*Churkina et al.*, 1999; *Nemani et al.*, 2002] because it is closely related to energy transfer processes. It also has applications in such areas as water resource management and wild fire assessment.

[3] As a result of historical efforts, accurate estimation of ET is becoming available via a number of methods using surface meteorological and sounding observations. However, the ground observation networks cover only a small portion of global land surface. Therefore many attempts have been made to minimize the use of ground observations for estimating spatial distribution of ET at regional to global scales. Satellite remote sensing is a promising tool for this purpose. Nevertheless, most of the existing techniques of ET estimation from satellite remote sensing are not satisfactory, because they still depend on ground observations. Therefore consistent estimation of up-to-date global ET distribution with satellite remote sensing independent of ground observations remains a challenging task. One possible approach is the utilization of the reanalysis data from global circulation model (GCM) as a surrogate for ground observations, but it is still problematic because the accuracy of the reanalysis also depends on the ground observation network. In addition, the grid scale of the reanalysis data is usually too coarse to be combined with finer scale satellite observations.

[4] One popular approach for estimation of ET from a satellite is using a combination of vegetation index (VI) and the surface radiant temperature (T_s). We call this approach the VI-T_s method. *Nemani and Running* [1989] showed the utility of a scatterplot of VI and T_s of a group of pixels inside a fixed square region (we call it "window") in a satellite image. Figure 1 is an illustration of VI-T_s scatter

0148-0227/03/2002JD002062$09.00

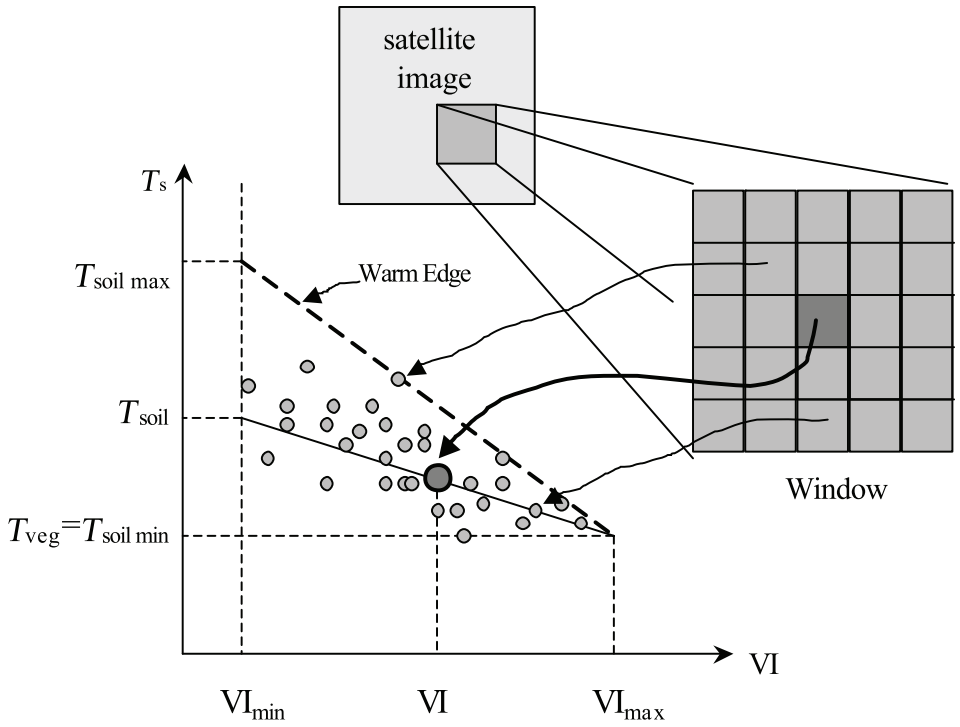

Figure 1. The VI-T_s diagram and the concept of estimation of $T_{soil\ max}$, T_{veg}, and T_{soil} for equation (27).

diagram. In general, a VI-T_s diagram shows a linear or triangular distribution with a negative correlation between VI and T_s. Changes in the slope of VI-T_s scatterplot (σ) during a growing season have been found to track modeled surface conductance in a semiarid ecosystem [*Nemani and Running*, 1989]. Generally speaking, σ assumes a negative value because dense vegetation (with high VI) has lower T_s. As the surface becomes drier, sparse vegetation and bare soil become warmer relative to vegetation resulting in larger negative values of σ.

[5] Since then, studies on VI-T_s methods made rapid progress. *Carlson et al.* [1995] and *Gillies et al.* [1997] established an inversion technique of their SVAT model to estimate available soil moisture (M_0) from VI-T_s triangle (named as the ''Triangle Method'') distributions without meteorological data. *Moran et al.* [1994] developed an algorithm to estimate ''water deficit index (WDI)'' through a simple geometric consideration on the VI-T_s diagram (which they call vegetation index-temperature trapezoid, VITT) with a theoretical basis of crop water stress index (CWSI) proposed by *Jackson et al.* [1981]. *Jiang and Islam* [2001] developed another VI-T_s method by linear decomposition of the triangular distribution of VI-T_s diagram and estimated the ''α'' parameter of the Priestley-Taylor's equation. This method has clear advantages of simplicity and consistency. It does not require any surface meteorology data.

[6] However, there are several difficulties to the above VI-T_s methods. First, some of them still need surface meteorological data. Second, inversion of numerical model may require large amount of computational resources when applied at global scales. Third, on a dense vegetation, T_s is close to the air temperature (T_a) because of small aerodynamic resistance of the vegetation canopy, making it difficult to estimate ET from a gradient of temperature. Fourth, some concepts are based on a single-source big-leaf model, which may be difficult to apply to complex landscapes with mixed land covers.

[7] In this study, we propose a new version of VI-T_s method for global ET estimation using moderate-resolution ($\sim$1 km) optical remote sensing data such as Aqua/MODIS sensor. Taking the above problems into account, we established five policies for the development of the proposed algorithm.

[8] (1) ''Stand alone.'' It can operate without surface meteorological data (e.g., wind speed, vapor pressure deficit (VPD), air temperature, boundary layer stability). In general, the VPD and the wind speed (or the aerodynamic resistance) are difficult to be estimated from remote sensing, yet critical for ET estimation. Therefore we tried to minimize the influence of these two meteorological elements in our algorithm.

[9] (2) ''Flexibility.'' If meteorological data are available, the algorithm should be flexible enough to incorporate them. It should also incorporate other ancillary data such as albedo, emissivity, and roughness when they are available. Therefore we must describe these variables explicitly in the algorithm.

[10] (3) ''Simplicity.'' It is simply constructed in order to save computational resources.

[11] (4) ''Scalability.'' It provides information not only about instantaneous but also about daily ET. This is because daily ET is more interesting for many users than instantaneous one. Moreover, because the NASA EOS project operates the two MODIS sensors onboard the EOS-AM (Terra) satellite and the EOS-PM (Aqua) satellite [*Running et al.*, 1994] and they observe each land surface twice a day (morning and afternoon), the algorithm should consistently process these multiple data sources if required.

[12] (5) "Versatility." It should operate regardless of the type of vegetation, land cover, season, and climate.

2. Algorithm

2.1. Evaporation Fraction (EF)

[13] We introduce "evaporation fraction (EF)" as an index for ET after *Shuttleworth et al.* [1989]:

$$\mathrm{ET} \equiv \mathrm{ET}/Q, \tag{1}$$

where Q is the available energy (W m^{-2}) which can be transferred directly into atmosphere as either sensible heat flux (H; in W m^{-2}) or latent heat flux. In other words,

$$Q \equiv H + \mathrm{ET}. \tag{2}$$

Because of energy conservation, we can also describe Q as the difference between the net radiation (R_n) and the ground heat transfer (G):

$$Q = R_n - G. \tag{3}$$

EF is directly related to the Bowen Ratio (= H/ET) by EF = 1/(1 + BR). However, we do not use BR because (1) BR is a nonlinear parameter for ET and (2) BR does not have upper limit (if ET approaches zero, BR goes to infinity).

[14] Our goal is estimation of EF rather than ET. This is due to three reasons: (1) EF is a suitable index for surface moisture condition, (2) EF is useful for temporal scaling, and (3) accurate estimation of Q is difficult. We explain each one of them hereafter.

[15] First, EF is more suitable index for surface moisture condition than ET. ET cannot be easily interpreted as an index for the soil moisture or drought status because it is a function not only of the surface moisture but some of the environmental factors such as the incoming radiation (or the available energy Q). On the contrary, EF is more directly related to the land surface conditions because of Q, the denominator of EF. Although in some exceptional cases ET may exceed Q (especially when a dry warm air mass flows onto a wet surface), Q is the possible upper limit of ET in most cases. Therefore dividing ET by Q results in a simple and rational way to represent the surface moisture condition or drought.

[16] Second, EF is useful for scaling instantaneous observations to longer time periods. Satellites (except the geostationary satellites) observe each land surface only a few times in a day. ET, however, generally shows large diurnal changes responding to the Sun angle and cloud coverage. Therefore even if we can estimate ET at the moment of satellite overpass, it cannot be directly related to the daily or daytime total ET. On the contrary, EF is nearly constant during most daytime in many cases [*Shuttleworth et al.*, 1989; *Sugita and Brutsaert*, 1991; *Crago*, 1996]. Therefore if we can estimate the daily or daytime average Q, we can estimate the daily or daytime average ET by using instantaneous EF derived by a satellite.

[17] Finally, accurate estimation of Q requires input data which are not easily available via optical remote sensing, such as atmospheric water vapor content and aerosol. Although we estimate Q during the process of estimating EF, we eventually normalize it in order to reduce errors because we cannot trust the accuracy of a simple radiative transfer algorithm of Q for a reliable estimation of ET.

[18] With reference to the first reason, we should further discuss "potential evaporation (PET)." PET is the maximum possible ET under specific climate and surface condition. Although many types of PET have been proposed, Penman's PET ($\mathrm{PET_{PM}}$; equation (4)) and Priestley and Taylor's PET ($\mathrm{PET_{PT}}$; equation (5)) [*Priestley and Taylor*, 1972] are the most widely accepted

$$\mathrm{ET_{PM}} = \frac{\Delta Q + \rho C_P (e_* - e)/r_a}{\Delta + \gamma} \tag{4}$$

and

$$\mathrm{ET_{PT}} = \frac{\alpha}{\Delta + \gamma} Q, \tag{5}$$

where Δ is derivative of the saturated vapor pressure in terms of temperature (Pa K^{-1}), γ is the psychrometric constant (Pa K^{-1}), ρ is the air density (kg m^{-3}), C_P is the specific heat of air under constant pressure (J kg^{-1} K^{-1}), e_* is the saturated vapor pressure (Pa) at the air temperature, e is the vapor pressure in the atmosphere (Pa), and r_a is the aerodynamic resistance (s m^{-1}). The VPD is $e_* - e$. The α in equation (5) is called "Priestley-Taylor's parameter." Although still controversial [e.g., *De Bruin*, 1983], 1.26 is generally accepted as the value of α.

[19] Because PET as well as Q set the upper limit of ET, PET can normalize ET and yield relative magnitude of ET. In fact, many studies use ET/PET instead of EF because PET represents a more realistic upper limit of ET than Q. For example, *Granger and Gray* [1989] used $\mathrm{ET/PET_{PM}}$ to see direct relationship between ET and VPD. *Choudhury et al.* [1994] used $\mathrm{ET/PET_{PT}}$ to see a relationship between vegetation index and ET. *Jiang and Islam* [2001] also used $\mathrm{PET_{PT}}$ as a normalization factor for ET. However, sometimes it is difficult to estimate PET as it requires meteorological information such as temperature, VPD, and wind speed. Therefore even if we get accurate value of ET/PET, it is difficult to convert it to the actual ET without such information. This is the main reason why we do not use ET/PET. The well-known diurnal stability of EF, which we mentioned previously, is another reason to use EF. The relation between EF and ET/PET is discussed in Appendix A as it played key role in the theoretical development of the algorithm.

2.2. Linear Two-Source Model of EF

[20] In our algorithm, we simplify a landscape as a mixture of two elements, namely, vegetation and bare soil. The proportion of vegetation is the fractional vegetation cover, namely, f_{veg} which takes a value between 0 and 1. Assuming a negligible coupled energy transfer between vegetation and bare soil, we describe ET from a pixel as a linear combination of ET from vegetation and ET from bare soil:

$$\mathrm{ET} = f_{\mathrm{veg}}\mathrm{ET_{veg}} + \left(1 - f_{\mathrm{veg}}\right)\mathrm{ET_{soil}}. \tag{6}$$

The subscripts "veg" and "soil" denote vegetation and bare soil, respectively. This linear model is invalid when ET varies significantly within each component. Such situation happens in a fragmented landscape with a markedly different surface temperature, moisture, and roughness between the two components [e.g., *Oke*, 1987]. Additionally, we can describe each of ET_{veg} and ET_{soil} by using EF:

$$ET_{veg} = Q_{veg}EF_{veg} \tag{7}$$

and

$$ET_{soil} = Q_{soil}EF_{soil}. \tag{8}$$

The difference between Q_{veg} and Q_{soil} comes from differences in thermal emission, solar reflectance, and ground heat flux between bare soil and vegetation. By dividing equation (6) with the available energy over the entire modeled landscape [$Q = f_{veg}Q_{veg} + (1 - f_{veg})Q_{soil}$] and using equations (7) and (8), we describe EF on the entire landscape (EF) as:

$$EF = \frac{ET}{Q} = f_{veg}\frac{Q_{veg}}{Q}EF_{veg} + (1 - f_{veg})\frac{Q_{soil}}{Q}EF_{soil}. \tag{9}$$

3. Estimation of Core Variables

[21] In equation (9), the most important variables (Core Variables) are f_{veg}, EF_{veg}, and EF_{soil}. In this section, we describe how to estimate these core variables. Most of the formulations of the core variables are not likely to change even if we get other ancillary data. However, in the estimation of the core variables, we need other variables such as air temperature, wind speed, incoming radiation etc. We call them as "basic variables" and they may be provided by other reliable data sources. We describe how we estimate the basic variables in section 4.

3.1. Fractional Vegetation Cover (f_{veg})

[22] The fractional vegetation cover (f_{veg}) is estimated from the spectral vegetation index. Although there are many types of vegetation indices, we can use normalized difference vegetation index (NDVI) as an example. NDVI is defined as a ratio of red (R_{red}) and near-infrared (R_{nir}) reflectances

$$NDVI = (R_{nir} - R_{red})/(R_{nir} + R_{red}). \tag{10}$$

If we can assume that NDVI is linearly related to f_{veg}, we can say:

$$f_{veg} = (NDVI - NDVI_{min})/(NDVI_{max} - NDVI_{min}), \tag{11}$$

where $NDVI_{max}$ and $NDVI_{min}$ are NDVI of full vegetation ($f_{veg} = 1$) and bare soil ($f_{veg} = 1$). The assumption of linearity of NDVI in terms of f_{veg} is not valid when the sum of two channels of reflectance ($R_{nir} + R_{red}$) is significantly different between vegetation and bare soil. We can minimize such influence by using advanced VIs such as SAVI [*Huete*, 1988] or EVI [*Huete et al.*, 1999] if some additional information is available.

3.2. Estimation of the EF of Vegetation (EF_{veg})

[23] Because of active turbulent diffusion, dense vegetation (especially forest) shows little difference between T_a and T_s regardless of the magnitude of ET. It makes estimation of ET difficult over dense vegetation using a temperature gradient (T_s-T_a) or some of the existing VI-T_s methods. The isolines of ET or soil moisture in such VI-T_s methods converge into one point at dense vegetation under the temperature gradient logic. In other words, from the standpoint of using temperature gradient, dense vegetation becomes a mathematically singular point. *Jiang and Islam* [2001] avoided this problem by assigning the maximum value of "α" parameter [i.e., $(\Delta + \gamma)/\Delta$] to the dense vegetation canopy assuming that the entire available energy is dissipated as ET over the dense vegetation. However, they are not always true because even a dense vegetation canopy responds to environmental conditions and does not always transpire at the potential rates. Therefore we have to consider physiology of the vegetation. For this reason, we introduce the surface resistance of the canopy in the formulation of EF_{veg} as follows.

[24] Let us consider ET_{veg} by using Penman-Monteith equation (12):

$$ET_{veg} = \frac{\Delta Q + \rho C_P(e_* - e)/r_a}{\Delta + \gamma(1 + r_c/r_a)}, \tag{12}$$

where r_c is surface resistance of the vegetation canopy (s m^{-1}). In this equation, the most difficult parameters to be obtained by a satellite are VPD (that is $e^* - e$) in the numerator and the wind speed, which controls r_a in both numerator and denominator. Therefore we want to minimize the influence of these two factors by modifying this equation. Dividing equation (12) by equation (4), we can remove the VPD term in the numerator to obtain:

$$\frac{ET_{veg}}{PET_{PM\,veg}} = \frac{\Delta + \gamma}{\Delta + \gamma(1 + r_c/r_a)}, \tag{13}$$

where $PET_{PM\ veg}$ is Penman's PET (equation (4)) on vegetation (W m^{-2}). Assuming the complementary relationship formulated by the *Brutsaert and Stricker*'s [1979] advection aridity (Appendix A), we can convert ET_{veg}/$PET_{PM\ veg}$ to EF_{veg} by solving equation (A5) and equation (13) and then get:

$$EF_{veg} = \frac{\alpha\Delta}{\Delta + \gamma(1 + r_c/2r_a)}. \tag{14}$$

Note that equation (14) becomes equivalent to Priestley-Taylor's PET (equation (5)) if r_c is zero. Although there is still an influence of VPD and wind speed in equation (14) because r_c depends on VPD and r_a depends on wind speed, the influence is less direct than equation (12). We use equation (14) to estimate EF_{veg} from satellite data.

[25] In this equation, Δ and γ are available from the air temperature T_a (although γ depends on atmospheric pres-

sure as well, the effect is usually small). We describe how to estimate T_a in section 4.1.

[26] We also need r_a and r_c to solve equation (14). In order to estimate r_a, we use the following empirical formulae [*Kondo*, 2000, 143 pp.; *Kondo*, 1994, 137 pp.]:

$$1/r_a = 0.008U_{50\,\mathrm{m}} \quad \text{for} \quad \text{forest canopy}, \tag{15}$$

$$1/r_a = 0.003U_{1\,\mathrm{m}} \quad \text{for} \quad \text{grassland and croplands}, \tag{16}$$

where $U_{50\ \mathrm{m}}$ and $U_{1\ \mathrm{m}}$ are wind speeds at 50 and 1.0 m heights, respectively (m s^{-1}).We estimate $U_{50\,\mathrm{m}}$ by using VI-T_s diagram, as described in section 4.3. We estimate $U_{1\ \mathrm{m}}$ from $U_{50\ \mathrm{m}}$ by using the logarithm profile of wind:

$$U = u_* \ln[(z-d)/z_0]/k, \tag{17}$$

where u_* is the shear velocity (m s^{-1}), z is the height (m), d is the surface displacement (m), z_0 is the roughness length (we assumed z_0 = 0.005 m for bare surface and 0.01 m for grassland after *Kondo* [2000]), and k is the von Karman's constant and we assume 0.4 as its value. Equation (17) is valid only under near-neutral condition. However, we can easily modify it if stability parameter (such as z/L; L is the Monin-Obukhov length) is available.

[27] For estimation of r_c in equation (13), we assume the environmental factors, namely temperature, VPD, photosynthetic active radiation (PAR), soil water potential, and atmospheric CO_2 concentration control stomatal conductance [*Jarvis*, 1976] in the following form:

$$1/r_c = f_1(T_a)f_2(\mathrm{PAR})f_3(\mathrm{VPD})f_4(\psi)f_5(\mathrm{CO_2})/r_{c\,\mathrm{MIN}} + 1/r_{\mathrm{cuticle}}, \tag{18}$$

where ψ is the leaf-water potential (Pa), $r_{c\ \mathrm{MIN}}$ is the minimum resistance (s m^{-1}), and r_{cuticle} is the canopy resistance related to diffusion through cuticle layer of leaves (s m^{-1}). Among the environmental factors in equation (18), only temperature and PAR can be estimated from satellite remote sensing and radiative transfer calculation, whereas VPD and ψ are hard to estimate from satellite data. However, some studies pointed out that temperature could sometimes be a surrogate for VPD. For example, *Tanaka et al.* [2000] reported in his field observation of deciduous conifer forest in Siberia that the behavior of the canopy conductance against VPD and temperature is mostly parallel to each other so that either one of them is sufficient to describe r_c. *Toda et al.* [2000] also reported a similar situation in a mixed landscape in Thailand where the distinctive rainy season and dry season exist. However, a severe soil water stress can often lead to a complete degradation of canopy. For example, *Hipps et al.* [1996] reported a rapid response of arid shrub foliages to soil water depletion in the Great Basin ecosystem. In such cases, change of f_{veg} (or vegetation index) and $\mathrm{EF_{soil}}$ should account for the drought. Therefore we decided to drop the terms of VPD, ψ, and CO_2 (f_2, f_4, and f_5) from equation (17) in the actual implementation although in some cases such simplifications may inevitably introduce large errors. However, if estimates of VPD become available from other data sources, we can easily incorporate them in equation (18).

Table 1. Parameters for the Canopy Conductance Mode

Abbreviation	Definition	Parameter
$R_{c\ \mathrm{MIN}}$	Minimum resistance (natural)	50 s m^{-1}
$R_{c\ \mathrm{MIN}}$	Minimum resistance (crop)	33 s m^{-1}
R_{cuticle}	Cuticle resistance	100,000 s m^{-1}
T_n,	Minimum temperature	2.7°C
T_o,	Optimal temperature	31.1°C
T_x	Maximum temperature	45.3°C
A	(Related to light use efficiency)	152 μmol m^{-2} s^{-1}

[28] We adopted the following equations [*Jarvis*, 1976; *Kosugi*, 1996] to estimate each of the components in equation (18):

$$f_1(T_a) = \left(\frac{T_a - T_n}{T_o - T_n}\right)\left(\frac{T_x - T_a}{T_x - T_o}\right)^{[(T_x - T_o)/(T_o - T_n)]}, \tag{19}$$

$$f_2(\mathrm{PAR}) = \frac{\mathrm{PAR}}{\mathrm{PAR} + A}, \tag{20}$$

where T_n, T_o, T_x are minimum, optimal, and maximum temperatures for stomatal activity, respectively. The parameter concerning photon absorption efficiency at low light intensity is A. These four parameters as well as $r_{c\ \mathrm{MIN}}$ determine the characteristics of the stomata behavior. Although they can change depending on species, structure of canopy, and adaptation to regional environment etc., we chose a set of representative values for all biomes for simplicity. We took the values of $r_{c\ \mathrm{MIN}}$ of *Kelliher et al.* [1995]. They showed that the maximum canopy conductance (reciprocal of $r_{c\ \mathrm{MIN}}$) of dense vegetation is approximately 2.7 times of maximum leaf conductance. They further concluded that the maximum canopy conductance is approximately 0.020 m s^{-1} (as a resistance, 50 s m^{-1}) for natural vegetation and 0.033 m s^{-1} (as a resistance, 33 s m^{-1}) for agricultural crops. For r_{cuticle}, we adopted the value used in Biome-BGC model [*White et al.*, 2000]. For T_n, T_o, T_x, and A, we adopted an experimental result of *Kosugi* [1996]. She determined these parameters for leaves of three tree species (*Quercus glauca*, *Cinnamomum camphora*, and *Pasania edulis*) without parameterization of VPD and ψ (f_2 and f_4). We took the average of each parameter in her experiment. Table 1 shows the settings of these parameters. Figure 2 shows dependency of $\mathrm{EF_{veg}}$ on temperature, wind speed, and vegetation types.

3.3. Estimation of EF at Bare Soil ($\mathrm{EF_{soil}}$)

[29] In order to estimate $\mathrm{EF_{soil}}$, we consider energy budget of a bare soil. First, we express the net radiation with radiation components as follows:

$$R_n = (1 - \mathrm{ref})R_d + L_d - \varepsilon\sigma T_s^4, \tag{21}$$

where ref is the albedo, R_d is the downward short-wave radiation (W m^{-2}), L_d is the downward long-wave (thermal infrared) radiation (W m^{-2}), ε is the emissivity, and σ is the

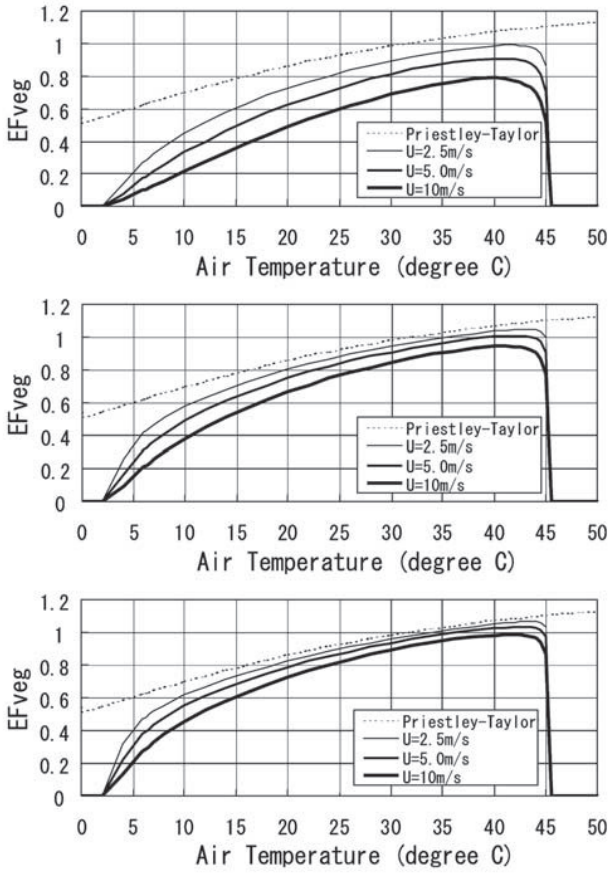

Figure 2. Dependency of EF_{veg} on air temperature, wind speed, and vegetation type. In these graphs, PAR was set to 1000 μmol m^{-2} s^{-1}. Broken lines are EF of Priestley-Taylor's PET, which is a limit of EF_{veg} with the canopy conductance close to zero or wind speed close to zero.

Stefan-Boltzmann constant (W m^{-2} K^{-4}). If we apply equation (21) to bare soil and expand the last term of equation (21) in terms of $T_{soil} - T_a$, we get $\varepsilon\sigma T_{soil}^4 \approx \varepsilon_{soil}\sigma T_a^4 + 4\varepsilon_{soil}\sigma T_a^3(T_{soil} - T_a)$. Then we can modify equation (21) to separate the effect of surface temperature and get:

$$R_n \approx R_{n0} - 4\varepsilon\sigma T_a^3(T_{soil} - T_a), \tag{22}$$

where $R_{n\,0}$ [$= (1 - \text{ref})R_d + L_d - \varepsilon\sigma T_a^4$] is the net radiation if T_{soil} is equal to T_a.

[30] Meanwhile, we can express the ground heat flux on a bare soil as:

$$G = C_G R_n, \tag{23}$$

where C_G is an empirical coefficient ranging from 0.3 for wet soil to 0.5 for dry soil [*Idso et al.*, 1975]. Then we can rewrite the energy budget (equation (3)) over bare soil:

$$Q_{soil} = R_n - G = (1 - C_G)R_n \approx (1 - C_G)\left[R_{n0} - 4\varepsilon\sigma T_a^3(T_{soil} - T_a)\right]$$

$$= H + \text{ET} = \rho C_P(T_{soil} - T_a)/r_{a\,soil} + \text{ET}. \tag{24}$$

From equation (24), we can then describe the surface temperature of bare soil as:

$$T_{soil} = \frac{Q_{soil\,0} - \text{ET}}{4\varepsilon\sigma T_a^3(1 - C_G) + \rho C_P/r_{a\,soil}} + T_a, \tag{25}$$

where $Q_{soil\ 0}$ [$= (1 - C_G)R_{n\ 0}$] is the available energy (W m^{-2}) when T_{soil} is equal to T_a. This equation means the surface temperature of bare soil is linearly related to ET as long as other variables are invariant. T_{soil} becomes the highest ($T_{soil\ max}$) if ET is zero:

$$T_{soil\ max} = \frac{Q_{soil\,0}}{4\varepsilon\sigma T_a^3(1 - C_G) + \rho C_P/r_{a\,soil}} + T_a. \tag{26}$$

By combination of equations (25) and (26), we get:

$$\frac{T_{soil\ max} - T_{soil}}{T_{soil\ max} - T_a} = \frac{\text{ET}_{soil}}{Q_{soil\,0}} = \frac{Q_{soil}}{Q_{soil\,0}}\text{EF}_{soil}. \tag{27}$$

In order to use equation (27) as a means to estimate EF_{soil}, we need to know the maximum possible temperature ($T_{soil\ max}$) and the actual temperature (T_{soil}) of bare soil as well as the air temperature (T_a). We evaluate them by using the VI-T_s diagram.

[31] If we can assume that a window for the VI-T_s diagram contains dry land surface, we can estimate the maximum possible temperature at bare soil ($T_{soil\ max}$) by looking at the left upper corner of the VI-T_s diagram (Figure 1). We can extrapolate the upper edge of the diagram to the minimum VI to estimate $T_{soil\ max}$. We call this upper edge the "warm edge" after *Carlson et al.* [1995]. This approach assumes that T_s can be described as a linear combination of surface temperature of vegetation cover and bare soil as:

$$T_s = f_{veg}T_{veg} + (1 - f_{veg})T_{soil}. \tag{28}$$

This is not true because the intensity of infrared radiation from the land surface (which is observable by satellite) depends on surface temperature in a nonlinear manner. However, as long as the difference between T_{veg} and T_{soil} is small in comparison to the absolute value of T_s (in K), equation (28) is approximately valid.

[32] Equation (27) may seem to be applicable to not only bare soil but also to any type of land surface, and in fact, *Moran et al.* [1994] took this approach in their VI-T_s algorithm (called "VITT"). However, we apply it to bare soil alone. This is because equation (27) assumes homogeneity of T_s and sensible heat transfer (H) inside a pixel. In other words, equation (27) is a single-source model. If the landscape is a mixture of vegetation and bare soil, we cannot define a representative temperature for a single source of sensible heat to derive equation (24). Additionally, if we apply equation (27) to a full vegetation canopy (replacing T_{soil} with T_{veg}), we can hardly estimate EF_{veg} because, as mentioned in section 3.2, the gradient of temperature over vegetation (especially forests) due to ET is much smaller in comparison to bare soil.

[33] It is important to note that equation (27) is only approximately valid because albedo (in $Q_{soil\ 0}$), emissivity

(ε), and C_G may change depending on soil water conditions. However, we assume their influences are small.

4. Estimation of Basic Variables

[34] EF and its core variables are dependent on the estimation of several basic variables, namely, air temperature (T_a), wind speed ($U_{50\ m}$), albedo (ref), available energy (Q), and PAR. In this section, we describe how we estimate them. Based on the policy of "flexibility," these basic variables may be replaced by other reliable data sources, such as ground observations, numerical model outputs, and other satellite remote sensing products.

4.1. Estimation of the Air Temperature (T_a)

[35] Because many studies reported that T_s of a full vegetation canopy (we call it T_{veg}) is close to the air temperature T_a [e.g., *Carlson et al.*, 1995; *Prince and Goward*, 1995], we assume them to be equal (i.e., $T_{veg} = T_a$). This is not true especially under extremely active or depressed ET. However, the magnitude of difference between these two temperatures is usually about 2 K [*Prince and Goward*, 1995] and we treat it as negligible in the estimation of Δ and γ in equation (13).

[36] In order to determine T_{veg}, we use the VI-T_s diagram (Figure 1) and *Prince and Goward*'s [1995] approach, which uses similar logic for the derivation of $T_{soil\ max}$. Taking the warm edge and extrapolating T_s value at the maximum VI, we interpret this extrapolated T_s as T_{veg}.

4.2. Estimation of the Albedo, Radiation Components, the Ground Heat Flux, and the Available Energy (Q)

[37] We need three kinds of available energy (Q_{veg}, Q_{soil}, and $Q_{soil\ 0}$) in equations (9) and (27) as well as the wind speed (section 4.3). Generally speaking, the available energy consists of the incoming short-wave radiation R_d, the reflected short-wave radiation R_u, the incoming long-wave radiation L_d, the outgoing long-wave radiation L_u, and the ground heat flux G. We describe each of them in the following.

[38] We estimated R_d using the radiative transfer scheme of *Kondo* [2000, pp. 299–306]. Because optical sensors on a satellite can observe the Earth surface only under a clear sky, we can assume that the turbidity and the precipitable water cannot be high when satellite data are available. Considering a common situation, we assumed 0.03 for turbidity, 0.20 for albedo, 60% for relative humidity, and 1013 hPa for standard atmospheric pressure for the radiative transfer calculation. However, we can substitute them with more realistic values when available.

[39] We estimated R_u by multiplying R_d with the albedo. We can approximate the albedo by averaging reflectance values for several visible and near-infrared channels observed by the satellite. This can introduce errors because channel reflectance values observed by a satellite are reflectance at only one Sun-target-sensor configuration and it is generally different from the albedo (hemispherical reflectance). But we assumed its influence to be small.

[40] The biggest error source is L_d in the estimation of the available energy. Accurate estimation of L_d requires an atmospheric profile of temperature and water vapor. Instead, we estimate L_d by assuming that the effective temperature of sky radiation is 20 K lower than T_a [*Kondo*, 1994].

[41] The outgoing long-wave radiation L_u can be estimated with T_s and the emissivity. Although the emissivity is difficult to estimate, the errors introduced to L_u by the emissivity are generally of an order of a few percent. Hence we assumed certain values of emissivity separately for vegetation and bare soil.

[42] Ground heat flux G of bare soil is estimated by equation (23) assuming certain value of C_G. Ground heat flux G of full vegetation is assumed to be negligible.

[43] PAR is estimated from R_d by multiplying a constant of 2.05 μmol W^{-1}.

4.3. Estimation of the Wind Speed ($U_{50\ m}$)

[44] Once we estimate T_a, $T_{soil\ max}$, and $Q_{soil\ 0}$, we can obtain aerodynamic resistance of bare soil ($r_{a\ soil}$) by solving equation (26). Then we convert it to wind speed by using the following empirical formula of aerodynamic resistance [*Kondo*, 1994, 137 pp.]:

$$1/r_{a\,soil} = 0.0015 U_{1\,m}. \tag{29}$$

We use equation (17) to convert $U_{1\ m}$ at bare soil to $U_{50\ m}$ assuming the roughness length of 0.005 m [*Kondo*, 2000, 143 pp.] and the surface displacement of 0 m. This goes to the estimation of r_a of vegetation (equations (15) and (16)) employed in equation (13).

[45] Figure 3 shows the flowchart of the algorithm to derive all the basic variables and the core variables from satellite data.

5. Prototype Development and Validation

5.1. Prototype Development

[46] We implemented this algorithm to create prototype data sets of EF. As inputs, we used NOAA/AVHRR 14-day composites over the continental United States with 1 km resolution from 1989 to 2000 provided by USGS EROS Data Center. All the data had been radiometrically calibrated including the effects of sensor degradation. Because NOAA-11 satellite failed in 1994, we excluded the year 1994 from the analysis. No atmospheric corrections were applied. We also used a land cover map generated by Global Land Cover Facility (GLCF) of University of Maryland [*Hansen et al.*, 2000] in order to classify forest, grassland, and cropland in the estimation of r_c and r_a. By using these data sets, we produced two kinds of prototypes of EF, namely, local prototypes at particular test sites and continental prototypes.

[47] We produced the local prototypes for the sake of validation of the algorithm through a comparison to ground observation data. We chose 13 test sites in the continental U.S. (Figure 4), each of which contained a flux tower of AmeriFlux project. We sought to compare the EF estimated by our algorithm with actually observed EF at these towers. Table 2 shows the details of each test site. For each test site, we extracted a window of 21 km × 21 m (with the flux tower site at the center) from the AVHRR composite data.

[48] We produced the continental prototypes in order to check the performance of the algorithm by looking at the

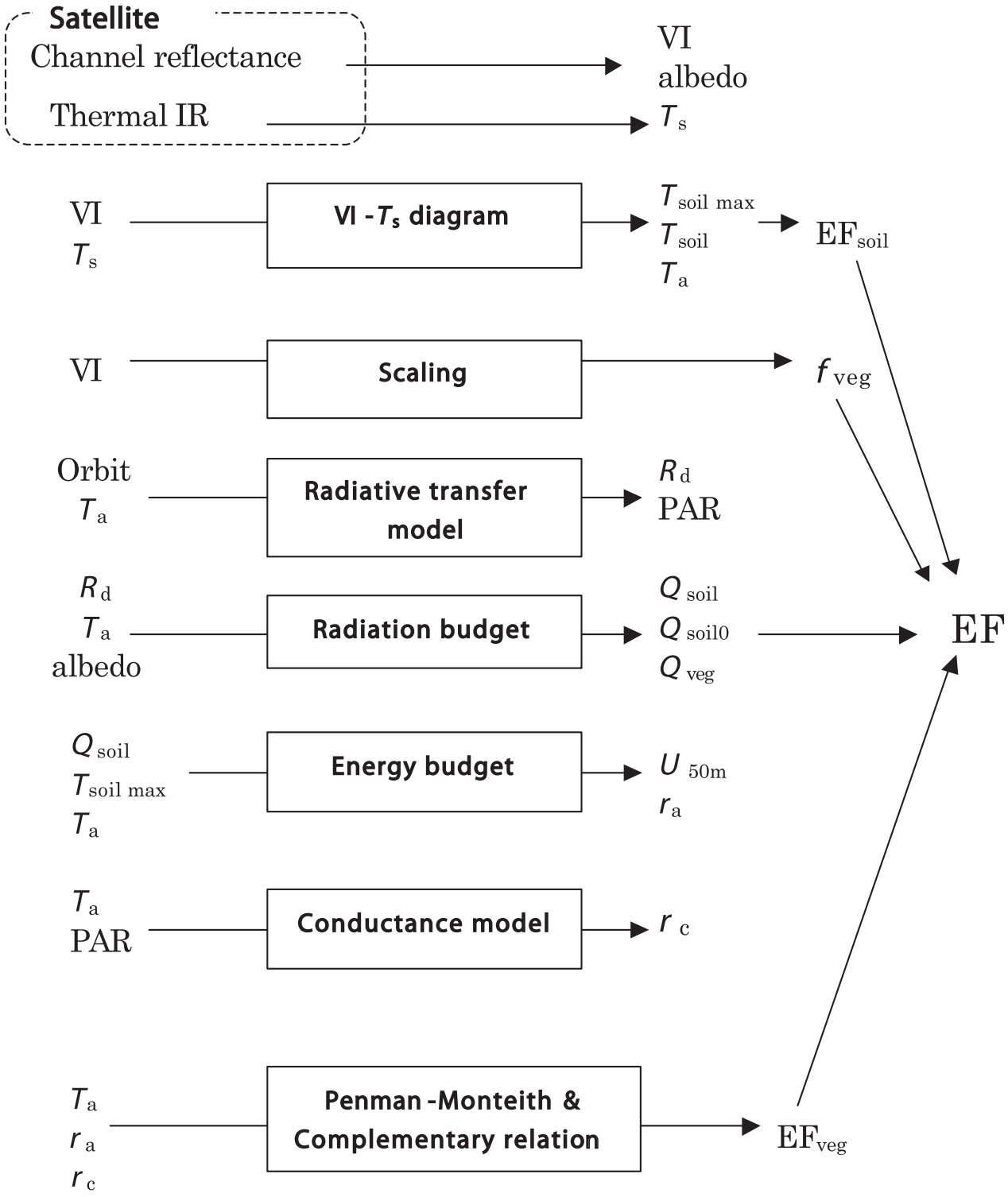

Figure 3. A flowchart of the process and variables in the algorithm. Each process (shown in a box) comes after the process above and its outputs go into the following processes.

spatial distribution of EF_{veg}, EF_{soil}, and EF. We used 26 composite scenes covering the entire year of 1997.

[49] Because of lack of some necessary information, we made further assumptions. We assumed the emissivity of all the pixels to be 0.98. This may be erroneous especially for dry bare soil. We also assumed the albedo as 0.2 for both bare soil and vegetation, because atmospheric correction for entire NOAA/AVHRR data was difficult and we could not

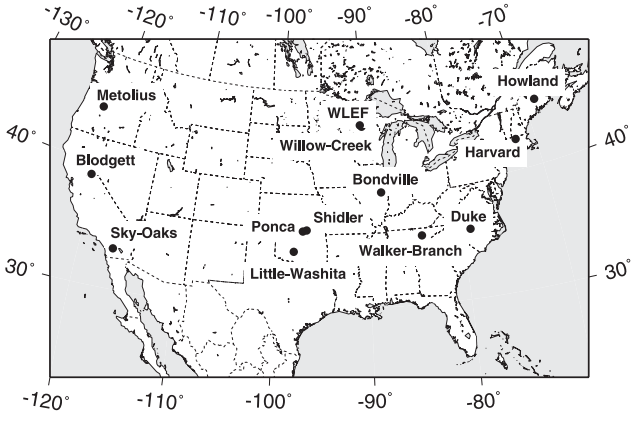

Figure 4. Locations of the test sites (AmeriFlux tower sites).

estimate albedo from channel reflectance data. We further assumed C_G to be 0.38. This is because *Moran et al.* [1989] proposed $C_G = 0.583 \exp(-2.13\text{NDVI})$. If we take 0.2 as the NDVI of bare soil, we get C_G as 0.38. Last, we assumed $\text{NDVI}_{\max}$ and $\text{NDVI}_{\min}$ for equation (11) as 0.75 and 0.2, respectively.

[50] We applied several quality checks to the AVHRR data set. First, we made cloud screening and BRDF screening (Appendix B). Then we calculated surface temperature (T_s) with a technique employed by *Thornton* [1998] using the split window method of *Coll et al.* [1994]. Then we imposed the following additional quality controls to get clear VI-T_s diagrams. We selected the pixels which were observed on the same day as the center pixel. This is because the VI-T_s diagram significantly changes from day to day due to changes of air temperature, wind speed etc., even during a week. After the quality checks, if the pixel number was reduced to below 44, 10% of the original size of the window, we discarded the entire data of that day for that test site.

[51] In order to obtain the "warm edge" on the VI-T_s diagram, we selected those pixels which are likely to be on the warm edge with the method of *Nemani et al.* [1993]. Then we calculated a linear regression line for those pixels and regarded it as the "warm edge." By substituting the values of $\text{NDVI}_{\max}$ and $\text{NDVI}_{\min}$ into the regression line, we obtained T_{veg} and $T_{\text{soil max}}$. We extrapolated a line from ($\text{NDVI}_{\max}$, T_{veg}) via (NDVI, T_s) of the center of the window to $\text{NDVI}_{\min}$ and obtained T_{soil} (see Figure 1).

5.2. Validation Data

[52] We prepared the validation data of EF from the data set of the each flux site. First, we interpolated the missing data of ET and H in the half-hourly flux data set for each site (WLEF tower site provided hourly data). If the number of missing exceeded 2 during a daytime period (0600 to 1800 hours), then we discarded the whole data of that day. We averaged ET and H for each daytime period and calculated daily daytime EF as ET/(ET + H). We discarded the nighttime data because nighttime ET could be an error source for estimating daily ET from instantaneous observation of EF [*Sugita and Brutsaert*, 1991]. Then we extracted the data on the same day of the satellite observation. Because the satellite data were biweekly, the useful data for the validation were only a small portion of the entire flux data sets.

5.3. Validation

[53] We compared the EF estimation in the local prototype and the EF validation data at each test site. In addition, in order to see the contribution of each part of our algorithm, and in order to investigate some shortcuts to save computational resources without losing accuracy, we tested some "simplified versions" of the algorithm. Because most of the complexity occurs in the estimation of EF_{soil} and EF_{veg}, we tested some simplifications of these two factors. For EF_{soil}, we tried two cases: (1) setting EF_{soil} to zero, and (2) the standard algorithm (section 3.3). For EF_{veg}, we tried three cases: (1) fixing EF_{veg} to 1.0, (2) setting EF_{veg} to $\alpha/(\Delta + \gamma)$ which is equivalent to Priestley-Taylor's PET, and (3) the standard algorithm (section 3.2). Therefore we tried six combinations of these settings. The simplest setting was $\text{EF}_{\text{soil}} = 0$ and $\text{EF}_{\text{veg}} = 1$. This setting is equivalent to estimating EF using VI alone. When we take the standard algorithm for EF_{soil} and set EF_{veg} to 1, it is similar to *Jiang and Islam*'s [2001] VI-T_s method (although

Table 2. Test Sites[a]

Name	Lat.	Long.	Year	Ecosystem	P.I.
Blodgett	38.89	−120.63	1997–1998	Ponderosa Pine	A. Goldstein
Bondville	40.05	−88.29	1997–1999	Corn/Soybean	T. Meyers
Duke Forest	35.978	−79.09	1998–1999	Loblolly Pine	R. Oren
Harvard Forest	42.5	−72.18	1992–1999	Oak-Maple	S. Wofsy
Howland	45.25	−68.75	1996–1999	Spruce-Hemlock	D. Hollinger
Little Washita	34.96	−97.98	1997–1998	Rangeland	T. Meyers
Metolius	44.5	−121.62	1996–1997	Ponderosa Pine	B. Law
Ponca	36.75	−97.08	1997	Wheat	S. Verma
Shidler	36.93	−96.68	1997	Tallgrass Prairie	S. Verma
Sky Oaks	33.36	−116.62	1997–1999	Shrub	W. Oechel
Walker Branch	35.958	−84.28	1995–1998	Oak-Hickory	K. Wilson
Willow Creek	45.817	−90.08	1998–1999	Hardwood	K. Davis
WLEF Tower	45.945	−90.28	1997–1999	Hardwood	P. Bakwin

[a]Note: "Lat." and "Lon." are latitude and longitude in decimal degrees, respectively. Latitude is positive in Northern Hemisphere. Longitude is negative in Western Hemisphere. In WLEF tower we used the flux data at 30 m height and interpolated hourly data into half-hourly. "P.I." means "principal investigator."

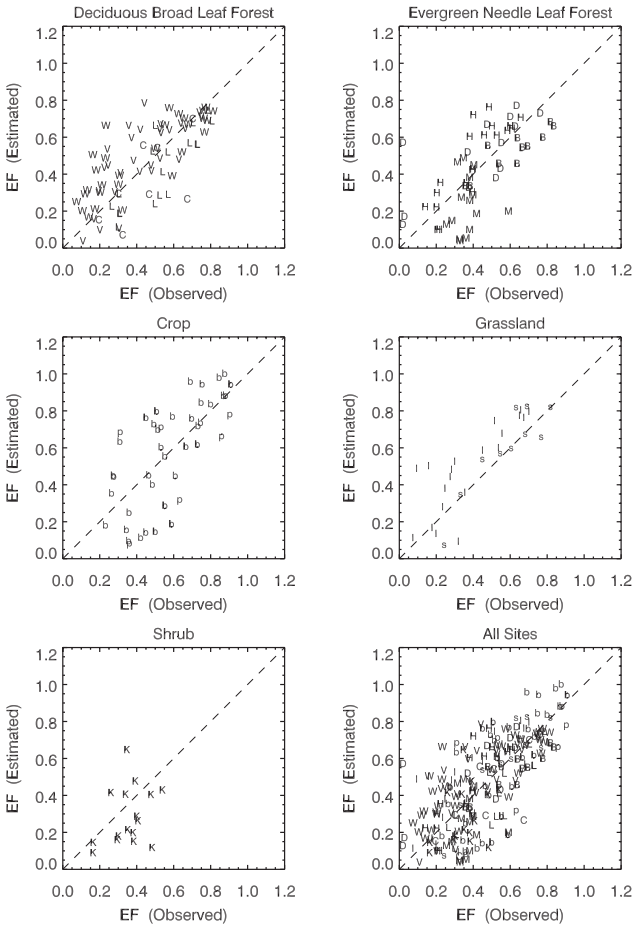

Figure 5. Comparison of the estimated EF by AVHRR and the observed EF at AmeriFlux sites, including Harvard Forest (V), Walker Branch (W), Willow Creek (C), WLEF Tower (L), Blodgett (B), Duke Forest (D), Howland (H), Metolius (M), Bondville (b), Ponca (P), Little Washita (l), Shidler (s), and Sky Oaks (K).

Table 3. Results of Validation of EF[a]

Site	Type	Data Size	R^2	Bias	Standard Error
Harvard Forest	DBF	28	0.74	0.06	0.15
Walker Branch	DBF	29	0.83	0.07	0.16
Willow Creek	DBF	8	0.63	−0.09	0.20
WLEF Tower	DBF	18	0.84	−0.11	0.15
Blodgett	ENF	11	0.89	−0.09	0.12
Duke Forest	ENF	13	0.72	0.09	0.20
Howland	ENF	20	0.85	0.08	0.14
Metolius	ENF	15	0.10	−0.13	0.21
Bondville	Crop	37	0.74	0.01	0.19
Ponca	Crop	6	0.45	−0.06	0.28
Little Washita	Grass	20	0.82	0.10	0.17
Shidler	Grass	10	0.90	0.01	0.11
Sky Oaks	Shrub	16	0.32	−0.07	0.17
All sites	...	231	0.71	0.01	0.17

[a]Note: DBF, deciduous broadleaf forest; ENF, evergreen needleleaf forest; R^2, correlation coefficient. "Bias" is average of difference between estimated EF and observed EF. "Standard error" is root mean square of difference between estimated EF and observed EF.

Table 4. Test of Simplified Versions of the Algorithm[a]

EF_{soil}	EF_{veg}	R^2	Bias	Standard Error
0	1	0.46	0.190	32
0	Priestley-Taylor	0.60	0.07	0.23
0	r_c model	0.70	−0.08	0.21
VI-T_s	1	0.50	0.28	0.36
VI-T_s	Priestley-Taylor	0.65	0.16	0.24
VI-T_s	r_c model	0.71	0.01	0.17

[a]Note: "VI-T_s" is the standard algorithm for EF_{soil}, whereas "r_c model" is the standard algorithm for EF_{veg}.

there are some differences such as in the method they used to determine the "warm edge").

6. Results and Discussions

[54] Figure 5 shows the comparison between the observed EF and the estimated EF (statistics in Table 3), with data distributed around the 1:1 line without a significant site bias. The large errors occurred in the croplands, whereas the grasslands showed relatively good accuracy. The overall standard error (the root mean square of the difference of observed EF and the estimated EF) was 0.18.

[55] Table 4 and Figure 6 show the performance of the "simplified versions" of the algorithm. The best algorithm

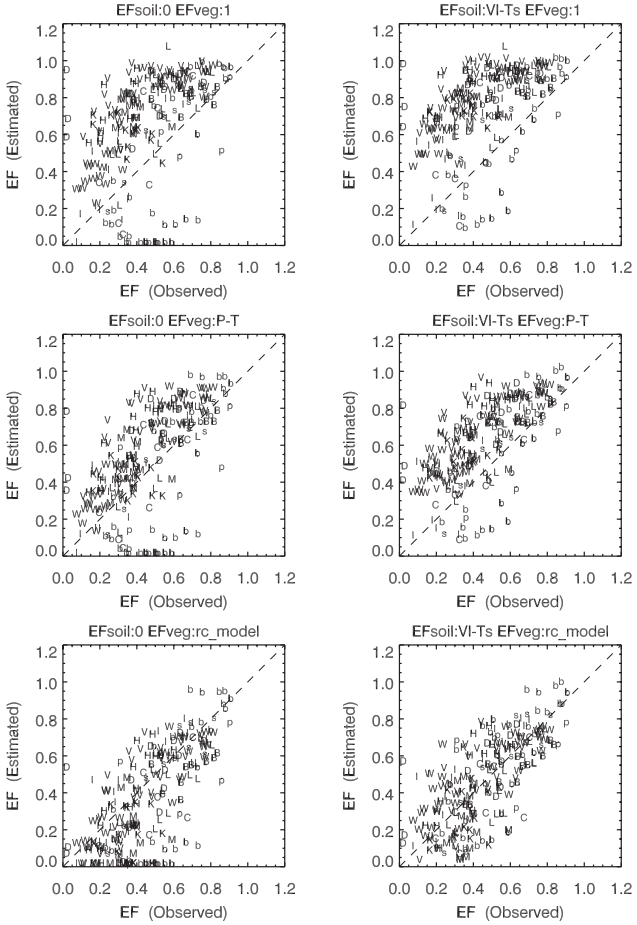

Figure 6. Observed and estimated EF with the simplified algorithms. Characters in the scatter graph correspond to the flux sites (see the caption of Figure 5).

Table 5. Results of Validation of Daytime ET (in W m^{-2})[a]

Site	Type	Data Size	R^2	Bias	Standard Error
Harvard Forest	DBF	28	0.81	25.01	58.45
Walker Branch	DBF	29	0.92	13.34	37.33
Willow Creek	DBF	8	0.92	−15.49	50.01
WLEF Tower	DBF	18	0.95	−15.61	29.16
Blodgett	ENF	11	0.97	−31.74	42.05
Duke Forest	ENF	13	0.92	15.11	32.76
Howland	ENF	20	0.91	26.90	47.75
Metolius	ENF	15	0.39	−27.76	53.72
Bondville	Crop	37	0.93	10.86	39.68
Ponca	Crop	6	0.75	6.01	85.91
Little Washita	Grass	20	0.95	24.68	35.85
Shidler	Grass	10	0.95	2.20	24.01
Sky Oaks	Shrub	16	0.51	−19.65	63.87
All sites	...	231	0.86	5.59	45.06

[a]Note: DBF, deciduous broadleaf forest; ENF, evergreen needleleaf forest; R^2, correlation coefficient. "Bias" is average of difference between estimated EF and observed EF. "Standard error" is root mean square of difference between estimated ET and observed ET. Estimation of ET is based on the estimated EF and the observed Q.

from a standpoint of accuracy was the standard algorithm for both EF_{soil} and EF_{veg}. Meanwhile, simplifying EF_{soil} to a fixed value of 0 did not result in a significant loss of accuracy. This implies that in many cases the soil evaporation was negligible within the accuracy of the prototype data set and the algorithm. Given the nature of satellite observations used, which were collected under an afternoon, clear-sky conditions, it is not surprising that soil evaporation played a negligible role. Because soil evaporation is largely controlled by water content of a thin layer at the surface and such a layer easily dries up quickly. Moreover, if leaf litter or dead woody materials cover the soil surface, the evaporation may be further reduced. In addition, bare soil is a relatively small component in many forested ecosystems and little energy transport occurs from the forest floor since the penetration of turbulent eddies and radiation are greatly reduced by the dense and tall canopy. This may explain the good performance of this simplification for the forests. On the contrary, this simplification showed relatively poor performance for the croplands, probably because the soil is more tightly coupled to the turbulent exchange and atmospheric conditions, especially under partial canopy cover. Meanwhile, the simplification of $EF_{veg} = 1$ introduced large errors to the EF estimation especially over forests. It implies that the explicit consideration of physiology was essential for the forests. On the other hand, grassland showed a good performance for this simplification. This may be due to the quick response of vegetation index to physiology of the grassland. The simplest setting (fixing $EF_{soil} = 0$ and $EF_{veg} = 1$) showed poor performance especially for forests. The simplified EF_{veg} by Priestley-Taylor's PET improved the accuracy in comparison to the case of $EF_{veg} = 0$, although not as much as standard algorithm.

[56] Table 5 and Figure 7 show the error of daytime ET calculated from the estimated EF and observed available energy Q. We found better R^2 values than that of the error of EF (Table 3). This is because most of ambiguous EF values happened under low available energy. Similar tendency has been reported for the Priestley-Taylor's alpha values estimated from NOAA/AVHRR data by *Jiang and Islam* [2001].

[57] The validity of linearity of NDVI and f_v (equation (11)) has been controversial [e.g., *Carlson and Ripley*, 1997]. However, if the denominator of equation (10), namely, the sum of the two channel reflectance values is the same between vegetation and bare soil, NDVI and f_v is related linearly. In order to see whether this was true in our data sets, we checked the NOAA/AVHRR data sets on each test site. We found that the sum of these two channel reflectance values showed little dependency on NDVI (at most 25% relative change). It means that the denominator of equation (10) was not very different between the vegetated pixels and the bare soil pixels in our data set. Therefore we believe the assumption of linearity of equation (11) could not be a major error source in this prototype study.

[58] Figure 8 shows an example of the continental-scale products. Although we can see some variability in EF_{soil} and EF_{veg} at the continental scale, the spatial distribution of the final product of EF is fairly similar to the distribution of the fractional vegetation cover. However, there are some regions which showed a considerable anomaly in EF in comparison to the fractional vegetation cover, such as Florida in the July scene or the south-central to northeastern region in the September scene. We also found that there was a wide area of missing pixels, probably due to clouds and/or unstable performance of the VI-T_s analysis.

[59] In terms of error assessment, one of the largest error sources is estimation of wind speed. In our prototype study, we found the average actual wind speed on the forest sites at the satellite overpass was 3.7 m s^{-1}, whereas the average estimated wind speed for these sites was 8.2 m s^{-1}. Meanwhile, the average actual wind speed on the nonforest sites at the satellite overpass

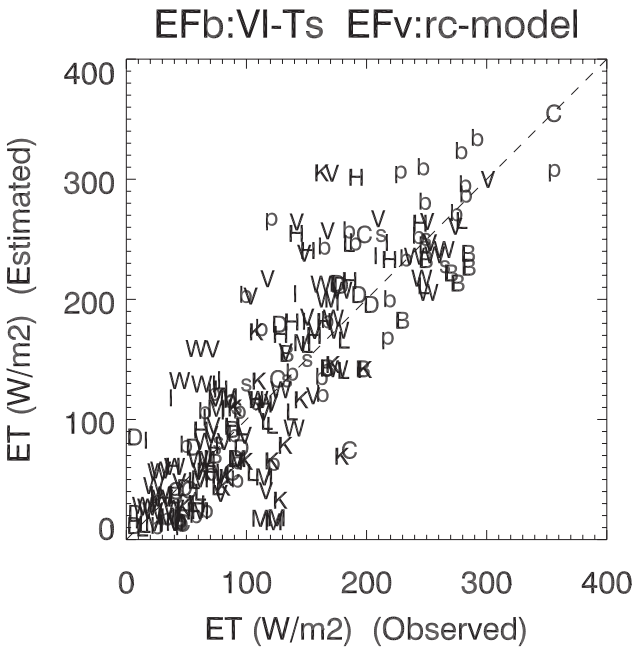

Figure 7. Comparison of the observed and estimated ET. Estimation of ET is based on the estimated EF and the observed Q. Characters in the scatter graph correspond to the flux sites (see the caption of Figure 5).

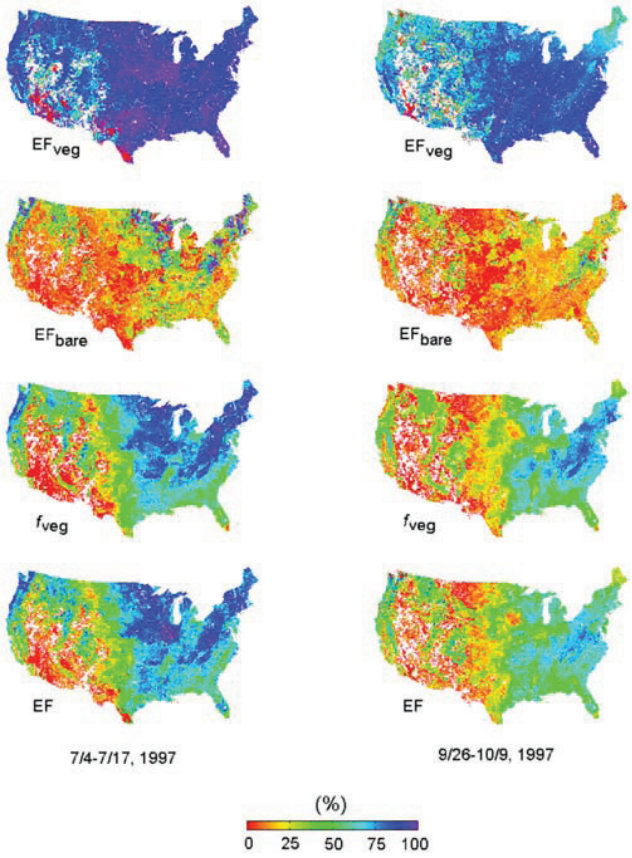

Figure 8. An example of the continental scale prototype of EF.

was 8.4 m s^{-1}, whereas the average estimated wind speed for these sites was 10.6 m s^{-1}. Such overestimation of the wind speed may be due to the erratic estimation of energy budget as well as unstable estimation of the maximum bare soil temperature on the VI-T_s diagram. It can influence the estimation of EF_{veg} as shown in Figure 2. In other words, we may expect improvement of accuracy of EF_{veg} by using Aqua/MODIS data which will hopefully give us better estimation of the albedo, the surface temperature, and the vegetation indices, all of which contributes to accuracy of the wind speed. Nevertheless, we may have to incorporate stability correction for the aerodynamic representation, especially under very stable or unstable conditions.

[60] Another problem is the influence of VPD and soil moisture on physiology. Because we did not incorporate these effects explicitly, they can sometimes translate to large errors. In fact, the performance of the prototype was not very good for dry ecosystems (Metolius and Sky Oak sites). One possible solution to this is the application of AIRS/MSU/HSB sensors. These sensors are deployed along with MODIS on the Aqua satellite and will produce the atmospheric profiles of humidity as well as temperature, with a horizontal spatial resolution of 50 km and a vertical resolution of 1000 m [*Chahine et al.*, 2001].

[61] Diurnal stability of EF is the key of the "scalability" policy. We tested it with the flux tower data. We took the difference between the instantaneous EF (observed during the 30 min of the satellite overpass) and the daytime EF (observed during the whole daytime period) at each site and found the root mean square of the difference was 0.090 (average among the sites). Although this is within the accuracy of the prototype, this can be dominant especially if the surface condition change drastically within a day.

[62] The concept of VI-T_s diagram is still controversial to some extent. First of all, different pixels have different vegetation, soil texture, and soil moisture content, irrespective of the fractional vegetation cover. In addition, each pixel has a slightly different set of atmospheric conditions above it. Therefore $T_{soil\ max}$ and T_{veg} values obtained from the diagram may not be physically meaningful for the entire scene.

[63] Another challenge in the VI-T_s concept is how to determine the warm edge or $T_{soil\ max}$. In our current approach, we estimate the warm edge from the observed VI-T_s diagram itself, under an assumption that there are pixels without soil evaporation inside the window. However, it is problematic if we do have the soil surface wet over all the pixels in the window. Such a situation is common in tropical areas during the rainy season. Even if there are some dry surfaces on the window, it may be difficult for coarse resolution sensors as AVHRR or MODIS to capture the warm edge if the dry surface is fragmented in a pixel. In this case, we may have to estimate $T_{soil\ max}$ from the energy budget (equation (26)). But it may be difficult because we need to estimate the aerodynamic resistance independently for equation (26). However, even if all pixels are wet, estimation of EF in vegetated pixels is still stable because EF is mostly derived from EF_{veg} which depends on temperature of the vegetated surface. On the other hand, another similar but different trouble can happen in homogeneously dry window such as desert. In this case, our EF algorithm becomes unstable because we cannot have accurate T_a from the diagram. We may need some backup algorithm for such case.

[64] A preliminary sensitivity analysis indicated $NDVI_{max}$ and $NDVI_{min}$ in equation (11) as the key parameters influencing EF estimation. It means that accurate MODIS vegetation indices may potentially improve the accuracy.

[65] A complete sensitivity analysis of the each variable and parameter is currently underway along with algorithm testing using Terra/MODIS data which will be extended to Aqua/MODIS.

7. Conclusion

[66] We developed an algorithm, to estimate EF (EF = ET/Q) by using optical satellite remote sensing, especially tailored to Aqua/MODIS sensor. The algorithm is a simple two-source model of ET in which we characterize a landscape as a mixture of bare soil and vegetation. In the estimation of EF of vegetation, we use the complementary relationship of the actual and the potential ET for the formulation of EF. In that, we use the canopy conductance model for describing vegetation physiology. On the other hand, we use "VI-T_s" (vegetation index-surface temperature) diagram for estimation of EF of bare soil. Although this algorithm requires only optical satellite data and a land classification map, it has the flexibility to

accept other data sources such as ground observations, numerical model outputs, or other satellite products, to improve its accuracy. We made the prototype products by using NOAA/AVHRR data sets and compared them with actual observations at 13 tower sites at a variety of geographic settings over the continental USA. As a result, the prototype products showed a standard error $\cong 0.18$ and $R^2 \cong 0.69$. Since our EF product is able to capture variations of surface energy partitioning and water exchange, it may help in several climatological and hydrological applications of remote sensing such as urbanization monitoring, water resource managements, and wild fire assessments along with large-scale climate and ecosystem dynamics.

Appendix A: Relationship Between EF and ET/PET

[67] According to equation (5), we obtain the relationship between ET/PET_{PT} and EF as:

$$\frac{ET}{PET_{PT}} = \frac{ET(\Delta+\gamma)}{Q_{soil0}} = \frac{\Delta+\gamma}{\alpha\Delta}EF. \quad (A1)$$

Because both Δ and γ mostly depend on temperature, we can convert EF to ET/PET_{PT} if temperature is available by using this equation.

[68] We assume complementary relationship [*Bouchet*, 1963; *Morton*, 1978] which says:

$$ET + PET = 2ET_0, \quad (A2)$$

where ET_0 is the ET when ET is equal to PET. *Brutsaert and Stricker* [1979] adopted PET_{PM} as PET and PET_{PT} as ET_0 in equation (A2). Then it comes to:

$$ET + PET_{PM} = 2ET_{PT}. \quad (A3)$$

We note that this formulation is controversial because it lacks theoretical background. For example, *Granger* [1989] theoretically proposed another form of the complementary relationship. According to the above equation, we can describe PET_{PM} as $2PET_{PT} - ET$. Therefore

$$\frac{ET}{PET_{PM}} = \frac{ET}{2PET_{PT} - ET} = \frac{ET/PET_{PT}}{2 - ET/PET_{PT}}. \quad (A4)$$

If we substitute ET/PET_{PT} by using equation (A1), we obtain:

$$\frac{ET}{PET_{PM}} = \frac{(\Delta+\gamma)EF}{2\alpha - (\Delta+\gamma)EF}. \quad (A5)$$

By using this equation, we can convert EF to ET/PET_{PM} under the assumption of the complementary relationship and the advection aridity.

Appendix B: Quality Control of AVHRR Data

[69] For the cloud screenings, we excluded pixels which satisfied at least one of the following four criteria (M. A. White and P. E. Thornton, personal communication, 2000):

$$R_2 > 35 \quad \text{and} \quad T_4 < 285\,\text{K}$$

$$R_2/R_1 < 1.2$$

$$T_4 - T_5 > 4.5\,\text{K} \quad \text{or} \quad T_4 - T_5 < -1.5\,\text{K}$$

$$T_3 - T_4 > 15\,\text{K} \quad (B1)$$

where R_1 and R_2 are reflectances of channels 1 and 2, whereas T_3, T_4, and T_5 are radiative brightness temperatures of channels 3, 4, and 5, respectively. In addition, we excluded those pixels which showed temporal decrease of NDVI value satisfying all of the following criteria.

$$NDVI_i < NDVI_{i-1}$$

$$NDVI_i < NDVI_{i+1}$$

$$\text{Max}(NDVI_{i+1} - NDVI_i,\ NDVI_{i-1} - NDVI_i) > 0.05. \quad (B2)$$

In order to avoid errors from low satellite elevation and hot spot of BRDF, we excluded the pixels which satisfied:

$$\theta < 15^\circ \quad \text{or} \quad \theta > 150^\circ \quad (B3)$$

where θ is an angle between the Sun-target-sensor.

[70] **Acknowledgments.** The following people are the principal investigators of AmeriFlux Project who provided us with their flux data for validation of our algorithm: Allen Goldstein (UC Berkeley), Walter Oechel (San Diego State University), Tilden Meyers (NOAA/ARL), Steve Wofsy (Harvard University), David Hollinger (USDA Forest Service), Ram Oren (Duke University), Shashi Verma (University of Nebraska), Beverly Law (Oregon State University), Kell Wilson (NOAA/ARL), Peter Bakwin (NOAA/OAR), and Kenneth Davis (Penn State University). We thank Michael A. White (Utah State University) and Peter E. Thornton (NCAR) for the cloud screening algorithm. This research was supported by Japan Society for the Promotion of Science (JSPS) Postdoctoral Fellowships for Research Abroad (fiscal year 1999–2001), the Biological and Environmental Research (BER) Program of U.S. Department of Energy through the Southeast Regional Center (SERC) of the National Institute for Global Environmental Change (NIGEC), and the Earth Science Division of NASA.

References

Bouchet, R. J., Evapotranspiration réele et potentielle, signification climatique, *Int. Assoc. Sci. Hydrol. Publ.*, *62*, 134–142, 1963.

Brutsaert, W., and H. Stricker, An advection-aridity approach to estimate actual regional evapotranspiration, *Water Resour. Res.*, *15*, 443–450, 1979.

Carlson, T. N., and D. A. Ripley, On the relation between Normalized Differential Vegetation Index, fractional vegetation cover, and leaf area index, *Remote Sens. Environ.*, *62*, 241–252, 1997.

Carlson, T. N., R. R. Gillies, and T. J. Schmugge, An interpretation of methodologies for indirect measurement of soil water content, *Agric. For. Meteorol.*, *77*, 191–205, 1995.

Chahine, M. T., H. Aumann, L. Goldberg, L. McMillin, P. Rosenkranz, D. Staelin, L. Strow, J. Susskind, and M. Gunson, AIRS-team retrieval for core products and geophysical parameters, AIRS Level 2 ATBD version 2.2, JPL D-17006, 2001.

Choudhury, B. J., N. U. Ahmed, S. B. Idso, R. J. Reginato, and C. S. T. Daughtry, Relations between evaporation coefficients and vegetation indices studied by model simulations, *Remote Sens. Environ.*, *50*, 1–17, 1994.

Churkina, G., S. W. Running, A. L. Schloss, and The Participants of the Potsdam NPP Model Intercomparison, Comparing global models of terrestrial net primary productivity (NPP): The importance of water availability, *Global Change Biol.*, *5*, suppl. 1, 46–55, 1999.

Coll, C., V. Caselles, J. A. Sobrino, and E. Valor, On the temperature dependence of the split-window equation for land surface temperature, *Int. J. Remote Sens.*, *48*, 127–134, 1994.

Crago, R. D., Comparison of the evaporative fraction and the Priestley-Taylor α for parameterizing daytime evaporation, *Water Resour. Res.*, *32*(5), 1403–1409, 1996.

De Bruin, H. A. R., A model for the Priestley-Taylor parameter α, *J. Clim. Appl. Meteorol.*, *22*, 572–578, 1983.

Gillies, R. R., T. N. Carlson, J. Cui, W. P. Kustas, and K. S. Humes, A verification of the "triangle" method for obtaining surface soil water content and energy fluxes from remote measurements of the Normalized Difference Vegetation Index (NDVI) and surface radiant temperature, *Int. J. Remote Sens.*, *18*(15), 3145–3166, 1997.

Granger, R. J., A complementary relationship approach for evaporation from nonsaturated surfaces, *J. Hydrol.*, *111*, 31–38, 1989.

Granger, R. J., and D. M. Gray, Evaporation from natural nonsaturated surfaces, *J. Hydrol.*, *111*, 21–29, 1989.

Hansen, M., R. DeFries, J. R. G. Townshend, and R. Sohlberg, Global land cover classification at 1 km resolution using a decision tree classifier, *Int. J. Remote Sens.*, *21*, 1331–1365, 2000.

Hipps, L. E., D. Or, and C. M. U. Neale, Spatial structure and scaling of surface fluxes in a Great Basin ecosystem, in *Scaling Up in Hydrology Using Remote Sensing*, edited by J. B. Stewart et al., pp. 113–125, John Wiley, New York, 1996.

Huete, A. R., A soil adjusted vegetation index (SAVI), *Remote Sens. Environ.*, *25*, 295–309, 1988.

Huete, A., C. Justice, and W. van Leeuwen, MODIS vegetation index (MOD13) algorithm theoretical basis document, version 3, 1999.

Idso, S. B., J. K. Aase, and R. D. Jackson, Net radiation—Soil heat flux relations as influenced by soil water content variations, *Boundary Layer Meteorol.*, *9*, 113–122, 1975.

Jackson, R. D., S. B. Idso, R. J. Reginato, and P. J. Pinter, Canopy temperature as a crop water stress indicator, *Water Resour. Res.*, *17*(4), 1133–1138, 1981.

Jarvis, P. G., The interpretation of the variations in leaf water potential and stomatal conductance found in canopies in the field, *Philos. Trans. R. Soc. London, Ser. B*, *273*, 593–610, 1976.

Jiang, L., and S. Islam, Estimation of surface evaporation map over southern great plains using remote sensing data, *Water Resour. Res.*, *37*(2), 329–340, 2001.

Kelliher, F. M., R. Leuning, M. R. Raupach, and E.-D. Schulze, Maximum conductance for evaporation from global vegetation types, *Agric. For. Meteorol.*, *73*, 1–16, 1995.

Kondo, J., *Meteorology of Water Environment*, 350 pp., Asakura-shoten, Tokyo, 1994.

Kondo, J., *Atmospheric Science Near the Ground Surface*, 324 pp., Univ. of Tokyo Press, Tokyo, 2000.

Kosugi, Y., Leaf-scale analysis of the CO_2 and H_2O exchange processes between trees and atmosphere, Ph.D. dissertation, Kyoto Univ., Kyoto, Japan, 1996.

Moran, M. S., R. D. Jackson, L. H. Raymond, L. W. Gay, and P. N. Slater, Mapping surface energy balance components by combining Landsat Thematic Mapper and ground-based meteorological data, *Remote Sens. Environ.*, *30*, 77–87, 1989.

Moran, M. S., T. R. Clarke, Y. Inoue, and A. Vidal, Estimating crop water deficit using the relation between surface-air temperature and spectral vegetation index, *Remote Sens. Environ.*, *49*, 246–263, 1994.

Morton, F. I., Estimating evapotranspiration from potential evaporation: Practicality of an iconoclastic approach, *J. Hydrol.*, *38*, 1–32, 1978.

Nemani, R. R., and S. W. Running, Estimation of regional surface resistance to evapotranspiration from NDVI and thermal-IR AVHRR data, *J. Appl. Meteorol.*, *28*, 276–284, 1989.

Nemani, R., L. Pierce, S. W. Running, and S. Goward, Developing satellite-derived estimates of surface moisture status, *J. Appl. Meteorol.*, *32*, 548–557, 1993.

Nemani, R. R., M. A. White, P. Thornton, K. Nishida, S. Reddy, J. Jenkins, and S. Running, Recent trends in hydrologic balance have enhanced the carbon sink in the United States, *Geophys. Res. Lett.*, *29*(10), 1468, doi:10.1029/2002GL014867, 2002.

Oke, T. R., *Boundary Layer Climates*, pp. 158–170, Routledge, New York, 1987.

Priestley, C. H. B., and R. J. Taylor, On the assessment of surface heat flux and evaporation using large-scale parameters, *Mon. Weather Rev.*, *100*, 81–92, 1972.

Prince, S. D., and S. N. Goward, Global primary production: A remote sensing approach, *J. Biogeogr.*, *22*, 815–835, 1995.

Running, S. W., et al., Terrestrial remote sensing science and algorithms planned for EOS/MODIS, *Int. J. Remote Sens.*, *15*(17), 3587–3620, 1994.

Shuttleworth, W. J., R. J. Gurney, A. Y. Hsu, and J. P. Ormsby, FIFE: The variation in energy partition at surface flux sites, *IAHS Publ.*, *186*, 67–74, 1989.

Sugita, M., and W. Brutsaert, Daily evaporation over a region from lower boundary-layer profiles measured with radiosondes, *Water Resour. Res.*, *27*(5), 747–752, 1991.

Tanaka, H., T. Ohta, T. Hiyama, and T. C. Maximov, Seasonal variation of photosynthesis and transpiration properties of a boreal deciduous forest: Analysis using a single layer canopy model, *J. Jpn. For. Soc.*, *82*(3), 259–267, 2000.

Thornton, P. E., Regional ecosystem simulation: Combining surface- and satellite-based observations to study linkages between terrestrial energy and mass budgets, Ph.D. dissertation, Univ. of Mont., Missoula, 1998.

Toda, M., N. Ohte, M. Tani, H. Tanaka, K. Musiake, M. Aoki, and S. Boonyawat, Diurnal and seasonal variations of CO_2 exchange processes over typical land covers in tropical monsoon region, *J. Jpn. Soc. Hydrol. Water Resour.*, *13*(4), 276–290, 2000.

White, M. A., P. E. Thornton, S. W. Running, and R. R. Nemani, Parameterization and sensitivity analysis of the BIOME-BGC terrestrial ecosystem model: Net primary production controls, *Earth Interact.*, *4*, paper 3, 85 pp., 2000.

J. M. Glassy, Lupine Logic, Inc., 131 West Spruce Street, Suite 3, Missoula, MT 59802, USA. (jglassy@lupinelogic.com)

R. R. Nemani and S. W. Running, Numerical Terradynamic Simulation Group (NTSG), School of Forestry, University of Montana, Missoula, MT 59812, USA. (nemani@ntsg.umt.edu; swr@ntsg.umt.edu)

K. Nishida, Institute of Agricultural and Forest Engineering, University of Tsukuba, 1-1-1 Tennoudai, Tsukuba, Ibaraki 305-8572, Japan. (kenlo@sakura.cc.tsukuba.ac.jp)